

Multilayer phoswich scintillators for neutron / gamma discrimination

Romain Coulon, Vladimir Kondrasovs, Quentin Lecomte, Jonathan Dumazert*

CEA, LIST, Laboratoire Capteurs et Architectures Electroniques, F-91191, Gif-sur-Yvette, France



ARTICLE INFO

Keywords:

Multilayer
Phoswich
Scintillators
Neutron
Gamma rays
Discrimination

ABSTRACT

MultiLayer Phoswich (MLP) scintillators have been studied for fission neutron detection by Monte-Carlo simulations and experimental tests. n/γ discrimination behavior of these systems and their angular dependencies have been characterized. The possibility to carry on a neutron counting system based of such an approach has been proven, and according to the results, an optimal thickness of layers for fission neutron counting was found around [100–150] μm . But, contrary to current liquid or solid-state discrimination scintillators, it appears that MLP-based neutron counting systems cannot directly classify neutron and gamma-ray interaction events from pulse shape analysis. To operate properly, it is therefore required to implement a compensation algorithm in the system readout.

1. Introduction

FISSION NEUTRON counting is a technique of interest for radio-protection purposes or for tackling radiological and nuclear threats. The challenge for this measurement is the recognition of neutron interactions from gamma-ray interactions. Liquid scintillation detector such as NE213 are today the most effective technology to address this issue (Cavallaro et al., 2013). Nevertheless, innovative techniques are still currently studied by research laboratories. We can mention thermal neutron detection using gadolinium or lithium converters (capture reactions) requiring the preliminary cooling of neutrons into a moderator (Dumazert et al., 2016, 2018; Cherepy et al., 2015), or plastic scintillators running with Triplet-Triplet Annihilation (TTA) process which attempt to face liquid scintillators (Zhmurin et al., 2014; Montbarbon et al., 2016). A less known technique based on multilayer scintillation system is investigated in this article.

Multilayer scintillation systems are currently employed in the field of space instrumentation (Batishev et al., 2015), medical physics (Lee et al., 2013), and fundamental physics research (Nakamura et al., 2006; Yu et al., 2017) to detect high-energy protons or high-energy neutrons. In 2011, the University of Kentucky envisaged a multilayer scintillation system to address fission neutron detection while underlying its potential capability to discriminate lower energy recoil protons compared with TTA solid-state scintillators (Kovash et al., 2011). The latter multilayer system was composed of organic scintillator layers with a specific optical insulation allowing each photomultiplier to detect the scintillation light from only one out of two foils. Assuming that recoil protons and recoil electrons from respectively neutron and gamma

incident particles do not have the same path length for a given energy, recoil protons are inclined towards releasing their kinetic energy in only one layer type, whereas recoil electrons tend to cross two layers. Thereafter, a coincidence event within the two channels would mean that a recoil electron from a gamma ray has crossed at least two adjacent layers, whereas an anti-coincidence event would indicate that a recoil proton from a fast neutron has ionized only one layer.

Based on this technology, the French Atomic Energy Commission (CEA) has proposed to develop an upgraded version of the multilayer scintillation system for fission neutron counting. The originality of the CEA's system relies on a phoswich configuration and its associated pulse shape discrimination technique. This MultiLayer Phoswich (MLP) scintillator is composed of layers having successively fast and slow decay fluorescence properties. These layers are linked with two photomultipliers working in coincidence mode allowing filtering a large part of thermionic pulses (dark noise) and thereby detecting low energy interaction events. Recorded coincident pulses are processed by a Pulse Shape Discrimination (PSD) algorithm, which estimates, for each of these interaction events, released energies into fast parts and into slow parts of the MLP. Fig. 1 illustrates this concept.

This article presents simulations and experimental tests of this MLP scintillator. The experimental setup will be firstly described, figures of merit will be established, and the calibration of the system will be detailed. Then, obtained results will be shaped and commented. Finally, a criticism and some perspectives of MLP scintillator for fission neutrons measurement will be proposed.

* Corresponding author.

E-mail address: jonathan.dumazert@cea.fr (J. Dumazert).

<https://doi.org/10.1016/j.radmeas.2018.07.011>

Received 4 April 2018; Received in revised form 15 June 2018; Accepted 16 July 2018

Available online 19 July 2018

1350-4487/ © 2018 Elsevier Ltd. All rights reserved.

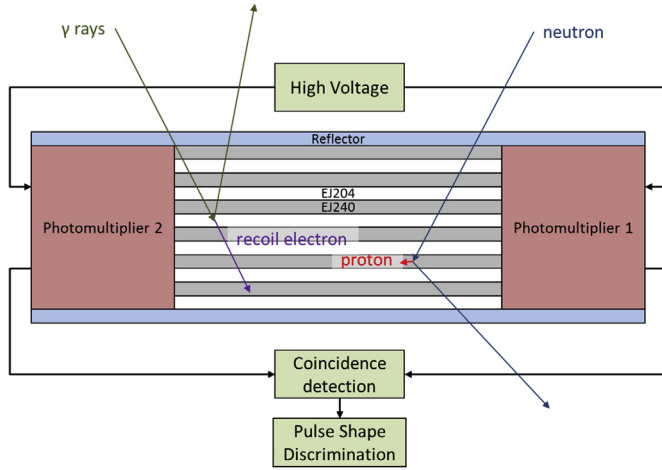


Fig. 1. Principle scheme of the MLP scintillator.

2. Material and method

2.1. Experimental setup

One of the aims of the study was to observe the behavior of MLP scintillators as a function of the incident angle θ of incident primary particles (γ or n) for different layer thicknesses ε . Fig. 2 presents nine configurations according to three angles: $\theta = \{0; 45; 90\}^\circ$ and three thicknesses: $\varepsilon = \{100; 200; 300\} \mu\text{m}$.

The MLP prototype is composed with 50×50 mm scintillation films from Eljen technology. Fast scintillator type is EJ204 with a decay time equal to 2 ns and a scintillation yield equal to 10400 photons per MeVee, whereas slow scintillator type is EJ240 with a decay time equal to 285 ns and a scintillation yield equal to 6300 photons per MeVee. The MLP scintillator is fixed on 2 mm-thick PMMA wave-guide and coupled with two super-Bialkali photomultipliers from Hamamatsu. A DT5743 from CAEN digitalized the signals from both channels with 3.2 GS.s^{-1} frequency and 12 bits resolution. Then, coincident pulses are triggered and recorded. The coincidence filtering reduces the dark noise magnitude by a factor of 230, allowing us to decrease the detection threshold, and to compensate the low photon-to-electron conversion efficiency. Thereafter, these pulses S_1 and S_2 are summed to obtain resulting pulses such as $S_3 = -(S_1 + S_2)$. A hypothesis test comparing the level of the derivative S' with the standard deviation $\sigma(S')$ associated with the baseline allows the localization of the signal start point

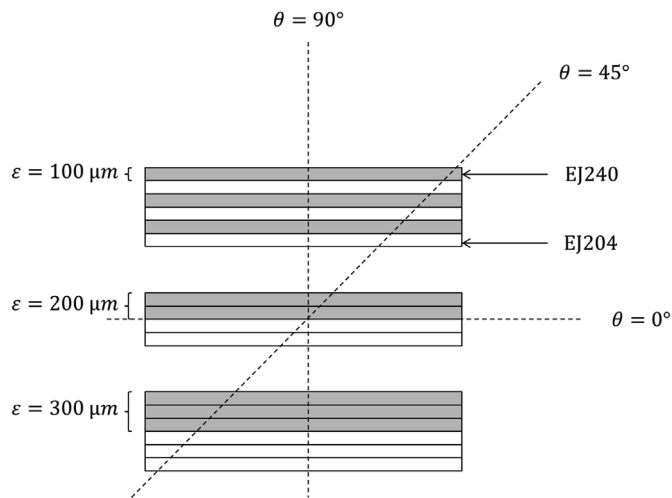


Fig. 2. Schematic view of the nine experimental configurations.

$\bar{\tau}_i$, such as:

$$\forall t \in \llbracket 1; n_t \rrbracket,$$

$$S'_t = S_{3,t+L} - S_{3,t-L} \quad (1)$$

$$\bar{\tau}_i = \arg_t (S'_t > q_\alpha \sigma(S'_t)) \quad (2)$$

where t is the time vector of length n_t (time window of recorded triggered pulses) defined in a discrete interval noted by $\llbracket \cdot \rrbracket$, L is the delay constant of the discrete derivative, $u \in \llbracket 1; 100 \rrbracket$ is a discrete time interval used to calculate the baseline, and q_α a coverage factor. The function $\arg_t(a > A)$ points out arguments of the vector a which are above the scalar value A .

Fast and slow charges are estimated by summing $S_{3,t}$ within respectively time interval $\bar{\tau}_i \leq t \leq \bar{\tau}_i + \Delta t$ and time interval $\bar{\tau}_i + \Delta t \leq t \leq n_t$, where Δt is an adjustable time window. The calibration factors k_f and k_s calibrate the energies E_f and E_s respectively deposited into the fast and the slow layers of the detector such as:

$$\begin{cases} E_f = k_f \sum_{t=\bar{\tau}_1}^{\bar{\tau}_1+\Delta t} S_{3,t} \\ E_s = k_s \sum_{t=\bar{\tau}_1+\Delta t}^{n_t} S_{3,t} \end{cases} \quad (3)$$

Spectra obtained by a gamma-rays source of ^{60}Co provide independent calibration factors k_f and k_s , and it must be emphasized that k_f is 1.64 times higher than k_s due to the scintillation yield gap between EJ204 and EJ240. section II.2 presents in detail this calibration. Subsequently, the total deposited energy E and the discrimination ratio R are calculated with following formulas:

$$\begin{cases} E = E_f + E_s \\ R = \frac{E_s}{E} \end{cases} \quad (4)$$

For each experimental configuration (cf. Fig. 2) and for each source type (^{60}Co and ^{252}Cf), n_p coincident pulses ($n_p > 100000$) are recorded by the CAEN DT5743 digitizer. Thereafter, each coincident pulse i is classified, according to its associated total released energy E_i and discrimination ratio R_i , into a discrimination matrix M , such as:

$$\forall i \in \llbracket 1; n_p \rrbracket,$$

$$\begin{cases} x_i = \arg_e (e = E_i) \\ y_i = \arg_r (r = R_i) \\ M_{x_i, y_i} = M_{x_i, y_i} + 1 \end{cases} \quad (5)$$

where e and r are discrete energy and discrimination ratio vectors of the discrimination matrix, and the function $\arg_a(a = A)$ points out the argument of the vector a which corresponds to the scalar value A . Additionally, the energy spectrum Y and the discrimination function Z are deduced from the matrix M such as:

$$\begin{cases} Y = \sum_{y=0}^{\infty} M_{x,y} \\ Z = \sum_{x=0}^{\infty} M_{x,y} \end{cases} \quad (6)$$

2.2. Energy calibration

The organic nature and small thickness of the scintillator make the observation of both the total absorption peak and the Compton edge impossible. This is why a MCNP6 model of the scintillation layers has been built, and deposited spectrum responses (tally f8) have been calculated and compared with experiments (Pelowitz et al, 2013a). Fig. 3 shows simulated and experimental spectra obtained for the irradiation by a ^{60}Co source obtained with a $100 \mu\text{m}$ -thick layer of EJ204. The k_f and k_s calibration parameters (cf. Eq. (3)) have been adjusted in order to fit the empirical spectrum with the full deposition trail of the

Download English Version:

<https://daneshyari.com/en/article/8249674>

Download Persian Version:

<https://daneshyari.com/article/8249674>

[Daneshyari.com](https://daneshyari.com)